# Dirichlet-to-Neumann map method for analyzing interpenetrating cylinder arrays in a triangular lattice

Yumao Wu,[1,2,3] and Ya Yan Lu[2]

[1]*Joint Advanced Research Center of University of Science and Technology of China and City University of Hong Kong, Suzhou, Jiangsu, China*

[2]*Department of Mathematics, City University of Hong Kong, Kowloon, Hong Kong*

[3]*Department of Mathematics, University of Science and Technology of China, Hefei, Anhui, China*

An efficient numerical method is developed for computing the transmission and reflection spectra of finite two-dimensional photonic crystals composed of circular cylinders in a triangular lattice. Our method manipulates a pair of operators defined on a set of curves and it remains effective when the radius of the cylinders is larger than $\sqrt{3}/4$ of the lattice constant — a condition where different arrays of cylinders cannot be separated by planes without intersecting the cylinders. The method is efficient since it never calculates the wave field in the interiors of the (hexagon) unit cells and it approximates the operators by small matrices. This is achieved by using the Dirichlet-to-Neumann (DtN) maps of the unit cells which map the wave field on the boundaries of the unit cells to its normal derivative. 

*OCIS codes:* 050.5298,000.4430

## 1. Introduction

Due to their unusual optical properties and significant potentials in applications, photonic crystals (PhCs) [1] have been extensively studied both theoretically and experimentally. Numerical simulations are essential to analyze basic properties of PhCs and to design PhC components for practical applications. The studies of PhCs give rise to a number of eigenvalue problems related to band structures and defect modes, as well as boundary value problems related to PhC components with various functions. For a PhC which is finite in one direction, it is important to compute its transmission and reflection spectra for plane incident waves. This leads to one of the simplest boundary value problems. Such a study is needed because

a PhC in practice must have a finite size. Meanwhile, the transmission and reflection spectra have close relationships with the band structures of the infinite PhC and they are related to experiments for testing theoretical calculations.

The mathematical formulation for plane wave scattering of a finite PhC is identical to that of the diffraction grating problem [2]. Therefore, existing numerical methods developed for diffraction gratings such as the Fourier modal method [3,4], the finite element method [5] and the integral equation methods [6], can be used to calculate the transmission and reflection spectra. However, these general methods are not the most efficient, since they fail to take advantage of the geometric features of the structure. For example, the Fourier modal method [3, 4] approximates a unit cell containing a simple circular cylinder by a multilayer structure using a staircase approximation to the material interface. The accuracy may be limited if the number of layers is not sufficiently large. For two-dimensional (2D) PhCs composed of circular cylinders (including both dielectric or metallic rods and air-holes) in a background medium, semi-analytic methods based on cylindrical wave expansions [7–12] are particularly efficient. In the multipole method [8], scattering matrices associated with one array of cylinders are first calculated by expanding the field in local polar coordinates of each cylinder in the array. Due to the infinite number of cylinders in the array, sophisticated lattice sums techniques are needed. The Dirichlet-to-Neumann (DtN) map method developed in [13–15] also uses cylindrical waves, but it does not require lattice sums, since the cylindrical waves are only used in a single unit cell to calculate its DtN map which maps the wave field on the boundary of the cell to its normal derivative. To separate different arrays of cylinders in a triangular lattice, the multipole method requires that $r < (\sqrt{3}/4)L$, where $a$ is the lattice constant and $r$ is the radius of the cylinders [16]. The DtN-map method developed in [14] requires the same condition, since it uses rectangular unit cells even for a triangular lattice.

In this paper, we develop an improved DtN-map method to overcome this limitation. Our method uses the DtN maps of hexagon unit cells and a generalized operator-marching technique for a pair of operators defined on curves. Our method is efficient because the DtN maps allow us to restrict the calculations to the edges of the unit cells and the operators are approximated by very small matrices due to an exponential convergence with respect to the number of points on each edge. We illustrate our method by a number of examples involving air-holes in a dielectric medium and dielectric or perfectly electric conductor cylinders in vacuum.

## 2. Problem formulation

We consider 2D PhCs composed of infinitely long parallel circular cylinders arranged as a triangular lattice in a homogeneous background medium. A typical example is shown in Fig. 1, where the refractive indices of the cylinders and the background medium are $n_1$ and

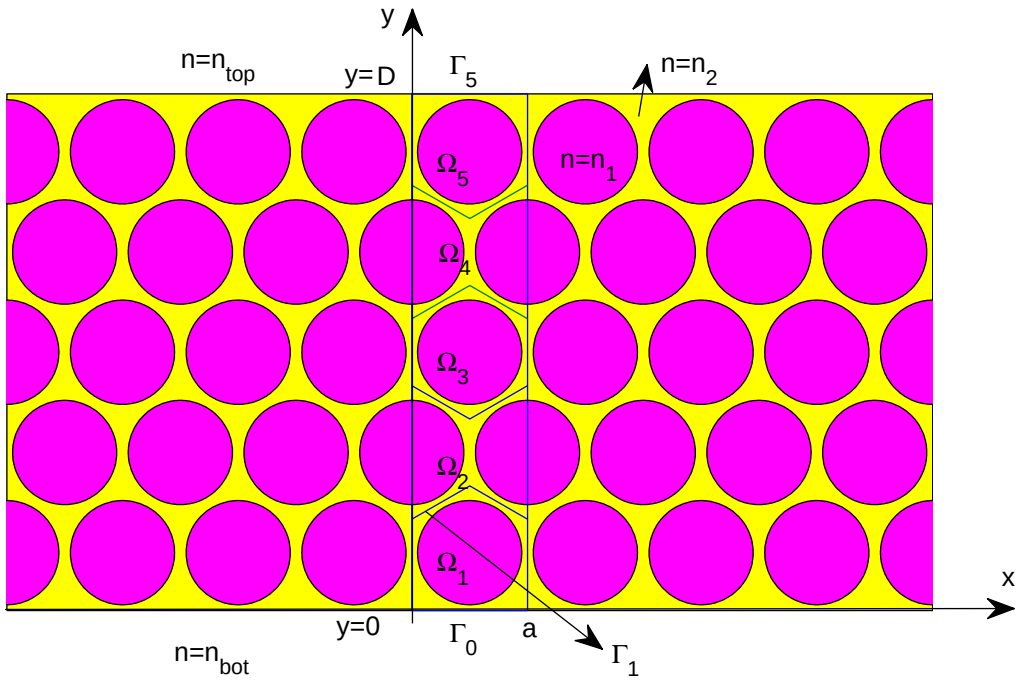


Fig. 1. A finite 2D photonic crystal with 5 interpenetrating arrays of circular cylinders. The refractive indices of the cylinders, the background medium, the media above and below are $n_1$, $n_2$, $n_{top}$ and $n_{bot}$, respectively. The domain $S$ covering one period in the horizontal direction is divided into 5 cells.

$n_2$, respectively. Let $x$ and $y$ be the horizontal and vertical coordinates corresponding to Fig. 1 and assume that the cylinders are parallel to the $z$-axis, then the structure is infinite and periodic in the $x$ direction with period $a$ ($a$ is also the lattice constant of the triangular lattice), and it is finite in the $y$ direction bounded by $y = 0$ and $y = D$ for a positive number $D$. For $y < 0$ and $y > D$, we have two homogeneous media with constant refractive indices $n_{bot}$ and $n_{top}$, respectively. For $0 < y < D$, the structure consists of a finite number of arrays of circular cylinders. We are particularly interested in the case where the radius $r$ of the cylinders satisfies $r > (\sqrt{3}/4)a$, so that the different arrays cannot be separated by horizontal planes of constant $y$ without intersecting the cylinders.

For waves propagating in the $xy$ plane only, we can separately consider the $E$ and $H$ polarizations. In the frequency domain, where the time dependence is assumed to be $\exp(-i\omega t)$ for an angular frequency $\omega$, the governing equation is the Helmholtz equation

$$p\frac{\partial}{\partial x}\left(\frac{1}{p}\frac{\partial u}{\partial x}\right) + p\frac{\partial}{\partial y}\left(\frac{1}{p}\frac{\partial u}{\partial y}\right) + k_0^2 n^2\, u = 0, \tag{1}$$

where $n = n(x, y)$ is the refractive index and $k_0$ is the free space wavenumber. For the $E$ polarization, $u$ is the $z$-component of the electric field and $p = 1$. For the $H$ polarization, $u$ is the $z$-component of the magnetic field and $p = n^2$.

Our problem is to study the reflection and transmission of a plane incident wave given in the top, i.e., $y > D$, as

$$u^{(i)}(x, y) = e^{i[\alpha_0 x - \beta_0 (y-D)]},$$

where $\beta_0$ is positive, $\alpha_0$ and $\beta_0$ satisfy $\alpha_0^2 + \beta_0^2 = k_0^2 n_{top}^2$. The total wave field $u$ is given as $u = u^{(i)} + u^{(r)}$ for $y > D$ and $u = u^{(t)}$ for $y < 0$. The reflected wave $u^{(r)}$ and the transmitted wave $u^{(t)}$ can be expanded in plane waves as

$$u^{(r)}(x, y) = \sum_{j=-\infty}^{\infty} R_j e^{i[\alpha_j x + \beta_j (y-D)]}, \quad y > D, \tag{2}$$

$$u^{(t)}(x, y) = \sum_{j=-\infty}^{\infty} T_j e^{i(\alpha_j x - \gamma_j y)}, \quad y < 0, \tag{3}$$

where $R_j$ and $T_j$ are the unknown reflection and transmission coefficients and

$$\alpha_j = \alpha_0 + \frac{2\pi j}{a}, \quad \beta_j = \sqrt{k_0^2 n_{top}^2 - \alpha_j^2}, \quad \gamma_j = \sqrt{k_0^2 n_{bot}^2 - \alpha_j^2}.$$

The problem can be formulated in the rectangular domain $S$ given by $0 < x < a$ and $0 < y < D$. Due to the periodicity of the structure in the $x$ direction and the $x$-dependence of the incident plane wave, the wave field is quasi-periodic in $x$, i.e., $u(x + a, y) = \rho\, u(x, y)$ for $\rho = \exp(i\alpha_0 a)$. This implies

$$u(a, y) = \rho\, u(0, y), \quad \frac{\partial u}{\partial x}(a, y) = \rho \frac{\partial u}{\partial x}(0, y). \tag{4}$$

With two properly defined operators $\tilde{S}_{top}$ and $\tilde{S}_{bot}$ [2, 13], we can write down the boundary conditions at $y = 0^-$ and $y = D^+$ as

$$\frac{\partial u}{\partial y} = -i\tilde{S}_{bot} u, \qquad y = 0^-, \tag{5}$$

$$\frac{\partial u}{\partial y} = i\tilde{S}_{top} u - 2i\beta_0 e^{i\alpha_0 x}, \quad y = D^+. \tag{6}$$

Therefore, we have a boundary value problem (1,4,5,6) for the Helmholtz equation.

## 3. Marching operators on curves

The DtN-map method developed in [13, 14] assumes that the domain $S$ given by $0 < x < a$ and $0 < y < D$, can be divided into a number of rectangular or square cells. More specifically, we have $y_j$, for $0 \le j \le m$, satisfying $0 = y_0 < y_1 < y_2 < ... < y_m = D$, so that the cells are $\Omega_j$ given by $0 < x < a$ and $y_{j-1} < y < y_j$, for $j = 1, 2, ..., m$. For cylinders in a triangular

lattice, if the radius of the cylinders satisfies $r < (\sqrt{3}/4)a$, then $y_j$ can be chosen so that the plane $y = y_j$ separates two arrays without intersecting the cylinders. In that case, the rectangular cell $\Omega_j$ either contains a single cylinder at its center or contains two half-cylinders where its vertical edges cut through the cylinders. It turns out that a cell with half-cylinders can be easily handled using the quasi-periodic condition. However, when $r > (\sqrt{3}/4)a$, the arrays interpenetrate and the plane $y = y_j$ intersects the cylinders. In that case, the method developed in [14] has difficulties.

In the following, we develop an improved DtN-map method for the case $r > (\sqrt{3}/4)a$. Our approach is to use hexagon unit cells for the bulk PhC and divide the domain $S$ into a number of cells as shown in Fig. 1. The cells $\Omega_1$, $\Omega_2$, ..., $\Omega_m$ are separated and bounded by two vertical lines at $x = 0$ and $x = a$, and the curves $\Gamma_j$ for $j = 0, 1, ..., m$. More precisely, $\Omega_j$ is bounded by $\Gamma_{j-1}$, $\Gamma_j$ and two vertical line segments at $x = 0$ and $x = a$. At the top and bottom, we still have straight lines, so that $\Gamma_0$ and $\Gamma_m$ are given by $y = 0$ and $y = D$, respectively. For $1 \le j < m$, the curve $\Gamma_j$ consists of two edges of the hexagon unit cells. The top and bottom cells, $\Omega_1$ and $\Omega_m$, are polygons having five edges, since $\Gamma_0$ and $\Gamma_m$ are straight lines. The cell $\Omega_j$ for $1 < j < m$, is either a hexagon unit cell of the bulk PhC or the union of two neighboring half-hexagons (which will be called a shifted hexagon). In the latter case, the vertical edges of $\Omega_j$ intersect with the cylinders. It will be explained in section 4 that such a cell can still be easily handled. For each point on the curve $\Gamma_j$, we also need a normal unit vector $\nu$, so that the normal derivative on $\Gamma_j$ can be defined. To be consistent with the $y$ derivative, we let the $y$-component of $\nu$ be positive. At a corner of $\Gamma_j$, $\nu$ is assumed to be the unit vector in the positive $y$ direction.

The DtN-map method developed in [13,14] employs an operator marching (OM) technique that manipulates two operators $Q_j$ and $Y_j$ defined on the line $y = y_j$. Here, we extend the definitions of these two operators to the curve $\Gamma_j$. For any solution $u$ of the Helmholtz equation (1) satisfying the quasi-periodic condition (4) and the bottom outgoing radiation condition (5), these two operators are required to satisfy

$$Q_j\, u|_{\Gamma_j} = \left.\frac{\partial u}{\partial \nu}\right|_{\Gamma_j}, \qquad Y_j\, u|_{\Gamma_j} = u|_{\Gamma_0}. \tag{7}$$

In the above, $Q_j$ is the global DtN operator which maps Dirichlet data on $\Gamma_j$ to Neumann data on $\Gamma_j$, and $Y_j$ is the fundamental solution (FS) operator that maps a function defined on $\Gamma_j$ to a function defined on $\Gamma_0$. On $\Gamma_0$ and $\Gamma_m$, since $n_{bot}$ and $n_{top}$ may be different from $n_2$ (the refractive index of the background medium for $0 < y < D$), we use the normal derivative of $u$ at $y = 0^+$ and $y = D^-$ to define $Q_0$ and $Q_m$, respectively. On an interior curve $\Gamma_j$ for $1 < j < m$, the normal derivative of $u$ is continuous for both polarizations. On $\Gamma_0$, we have

$$Q_0 = -i\delta_0 \tilde{S}_{bot}, \qquad Y_0 = I, \tag{8}$$

where $I$ is the identity operator, $\delta_0 = 1$ or $\delta_0 = n_2^2/n_{bot}^2$ for the $E$ or $H$ polarizations, respectively. These results are obtained from the boundary condition (5) and the definition of $Y$. For the $H$ polarization, the first equation of (8) is derived from

$$\left.\frac{1}{n_{bot}^2}\frac{\partial u}{\partial y}\right|_{y=0^-} = \frac{-i}{n_{bot}^2}\tilde{S}_{bot}\, u|_{y=0} = \left.\frac{1}{n_2^2}\frac{\partial u}{\partial y}\right|_{y=0^+} = \frac{1}{n_2^2}Q_0\, u|_{y=0}.$$

The DtN-map method then marches the operators from $\Gamma_{j-1}$ to $\Gamma_j$. After the two operators on $\Gamma_m$, i.e., $Q_m$ and $Y_m$, are obtained, we can calculate the total wave field at $y = D$ from the boundary condition (6), that is

$$[\delta_m Q_m - i\tilde{S}_{top}]\, u(x, D) = -2i\beta_0 e^{i\alpha_0 x}, \tag{9}$$

where $\delta_m = 1$ or $\delta_m = n_{top}^2/n_2^2$ for the $E$ or $H$ polarizations, respectively. For the $H$ polarization, Eq. (9) is derived from

$$\left.\frac{1}{n_2^2}\frac{\partial u}{\partial y}\right|_{y=D^-} = \frac{1}{n_2^2}Q_m\, u|_{y=D} = \left.\frac{1}{n_{top}^2}\frac{\partial u}{\partial y}\right|_{y=D^+} = \frac{1}{n_{top}^2}\left[i\tilde{S}_{top}\, u|_{y=D} - 2i\beta_0 e^{i\alpha_0 x}\right].$$

The reflected wave $u^{(r)}$ is then obtained by subtracting the incident wave from the total wave field:

$$u^{(r)}(x, D^+) = u(x, D) - u^{(i)}(x, D^+) = u(x, D) - e^{i\alpha_0 x}. \tag{10}$$

Meanwhile, the FS operator at $y = D$, i.e., $Y_m$, gives us the transmitted wave $u^{(t)}$:

$$u^{(t)}(x, 0^-) = u(x, 0) = Y_m\, u(x, D). \tag{11}$$

To march the operators from $\Gamma_{j-1}$ to $\Gamma_j$, that is, to calculate $Q_j$ and $Y_j$ from the given $Q_{j-1}$ and $Y_{j-1}$, we need the operator $M_j$ satisfying

$$M_j \begin{bmatrix} u_{j-1} \\ u_j \end{bmatrix} = \begin{bmatrix} M_{11} & M_{12} \\ M_{21} & M_{22} \end{bmatrix} \begin{bmatrix} u_{j-1} \\ u_j \end{bmatrix} = \begin{bmatrix} \partial_\nu u_{j-1} \\ \partial_\nu u_j \end{bmatrix}, \tag{12}$$

where $u$ is any solution of the Helmholtz equation (1) satisfying the quasi-periodic condition (4), $u_j$ and $\partial_\nu u_j$ denote $u$ and $\partial_\nu u$ evaluated on $\Gamma_j$, etc. Since the operator $M_j$ maps Dirichlet data to Neumann data on the two curves, it is also a DtN map. We call $M_j$ the reduced DtN map of $\Omega_j$, since the two vertical edges of $\Omega_j$ are not involved. In (12), the operator $M_j$ is given in a $2 \times 2$ block matrix form. This implies that $M_{11}$ maps a function defined on $\Gamma_{j-1}$ to a function defined on $\Gamma_{j-1}$, $M_{12}$ maps a function defined on $\Gamma_j$ to a function defined on $\Gamma_{j-1}$, etc. Replacing $\partial_\nu u_j$ and $\partial_\nu u_{j-1}$ by $Q_j u_j$ and $Q_{j-1} u_{j-1}$ in (12), respectively, we have

$$(Q_{j-1} - M_{11})u_{j-1} = M_{12}u_j, \quad M_{21}u_{j-1} = (Q_j - M_{22})u_j.$$

We can solve $u_{j-1}$ from the first equation, then insert the result into the second equation. The obtained relation is supposed to be valid for any solution of (1), (4) and (5). Therefore, we have

$$Q_j = M_{22} + M_{21}(Q_{j-1} - M_{11})^{-1}M_{12}, \tag{13}$$

$$Y_j = Y_{j-1}(Q_j - M_{11})^{-1}M_{12}. \tag{14}$$

## 4. DtN and reduced DtN maps of unit cells

In this section, we describe our method for computing the reduced DtN map $M_j$. First, we assume that the cell $\Omega_j$ contains a circular cylinder as shown in Fig. 2. To find $M_j$, we first construct its DtN map $\Lambda_j$ which maps $u$ on the boundary of $\Omega_j$ to the normal derivative of

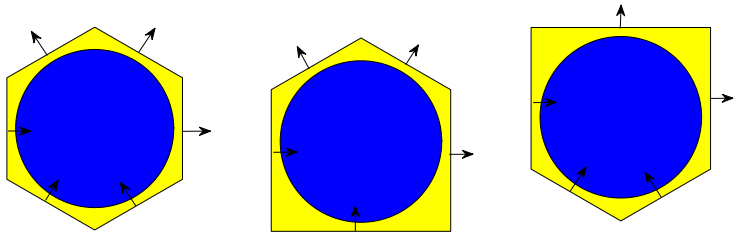

Fig. 2. Hexagon unit cell for a triangular lattice (left) and polygon cells (middle and right) near the edges of a finite photonic crystal, each containing one circular cylinder. A unit normal vector is also shown on each edge of the cells.

$u$ (also on the boundary of $\Omega_j$) for any $u$ satisfying the Helmholtz equation (1). The cell $\Omega_j$ is bounded by curves $\Gamma_{j-1}$, $\Gamma_j$ and two vertical edges at $x = 0$ and $x = a$. In the previous section, we have already chosen the unit normal vector $\nu$ on $\Gamma_j$, for $0 \le j \le m$, such that the $y$-component of $\nu$ is positive. For the vertical edges, we choose $\nu$ to be the unit vector in the $x$ direction. Therefore, $\Lambda_j$ satisfies

$$\Lambda_j \begin{bmatrix} u_{j-1} \\ w_0 \\ w_1 \\ u_j \end{bmatrix} = \begin{bmatrix} \Lambda_{11} & \Lambda_{12} & \Lambda_{13} & \Lambda_{14} \\ \Lambda_{21} & \Lambda_{22} & \Lambda_{23} & \Lambda_{24} \\ \Lambda_{31} & \Lambda_{32} & \Lambda_{33} & \Lambda_{34} \\ \Lambda_{41} & \Lambda_{42} & \Lambda_{43} & \Lambda_{44} \end{bmatrix} \begin{bmatrix} u_{j-1} \\ w_0 \\ w_1 \\ u_j \end{bmatrix} = \begin{bmatrix} \partial_\nu u_{j-1} \\ \partial_x w_0 \\ \partial_x w_1 \\ \partial_\nu u_j \end{bmatrix}, \tag{15}$$

where $u_{j-1}$, $u_j$, $w_0$ and $w_1$ denote $u$ on $\Gamma_{j-1}$ and $\Gamma_j$, on the vertical edges at $x = 0$ and $x = a$, respectively, $\partial_\nu u_{j-1}$, $\partial_\nu u_j$, $\partial_x w_0$ and $\partial_x w_1$ denote the corresponding normal derivatives of $u$. To obtain a matrix approximation of $\Lambda_j$ [13, 17], we choose $K$ sampling points on the boundary of $\Omega_j$ (avoiding the corner points of $\Omega_j$) and approximate the general solution of

Eq. (1) in $\Omega_j$ by a superposition of $K$ special solutions:

$$u(\mathbf{x}) \approx \sum_{k=1}^{K} c_k \phi_k(\mathbf{x}), \quad \text{for} \quad \mathbf{x} = (x, y). \tag{16}$$

For a cell containing a circular cylinder, the special solutions $\phi_k$ are known analytically as the cylindrical waves. The DtN map $\Lambda_j$ is then approximated by a $K \times K$ matrix. Let $\mathbf{x}_l$ (for $1 \le l \le K$) be the $K$ sampling points on the boundary of $\Omega_j$, we can calculate two $K \times K$ matrices $\mathcal{A}$ and $\mathcal{B}$ whose $(l, k)$ entries are $\phi_k(\mathbf{x}_l)$ and $\partial\phi_k(\mathbf{x}_l)/\partial\nu(\mathbf{x}_l)$, respectively. Then, the matrix approximation of the DtN map is

$$\Lambda_j = \mathcal{B}\mathcal{A}^{-1}.$$

More details can be found in [13, 17].

Once $\Lambda_j$ is obtained, we can construct the reduced DtN map $M_j$ using the quasi-periodic condition (4). In Eq. (15), the DtN map $\Lambda_j$ is given in $4 \times 4$ blocks. From the quasi-periodic condition (4), we have $w_1 = \rho w_0$ and $\partial_x w_1 = \rho \partial_x w_0$ for $\rho = \exp(i\alpha_0 a)$. These conditions can be used to eliminate $w_0$ and $w_1$ in (15). We obtain

$$M_j = \begin{bmatrix} \Lambda_{11} & \Lambda_{14} \\ \Lambda_{41} & \Lambda_{44} \end{bmatrix} + \begin{bmatrix} C_1 D_1 & C_1 D_2 \\ C_2 D_1 & C_2 D_2 \end{bmatrix}, \tag{17}$$

where $C_1$, $C_2$, $D_1$ and $D_2$ are matrices given by

$$\begin{aligned} &C_1 = \Lambda_{12} + \rho\Lambda_{13}, \quad C_2 = \Lambda_{42} + \rho\Lambda_{43}, \\ &D_0 = \rho\Lambda_{22} + \rho^2\Lambda_{23} - \Lambda_{32} - \rho\Lambda_{33}, \\ &D_1 = D_0^{-1}(\Lambda_{31} - \rho\Lambda_{21}), \quad D_2 = D_0^{-1}(\Lambda_{34} - \rho\Lambda_{24}). \end{aligned}$$

Next, we consider cells that contain two half-cylinders as in Fig. 3. For such a cell $\Omega_j$, it

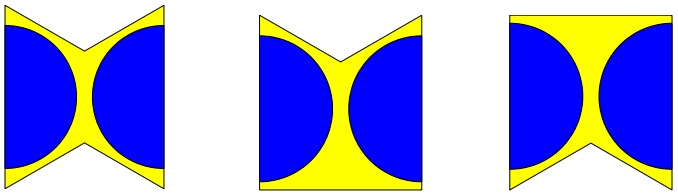

Fig. 3. Shifted cells corresponding to the hexagon unit cell and the polygon cells in Fig. 2, each containing two half-cylinders.

is not necessary to find its DtN map $\Lambda_j$. Instead, we can calculate the reduced DtN map

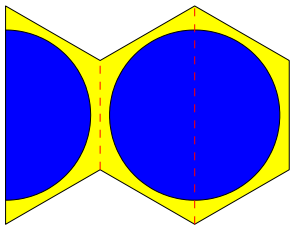

Fig. 4. A shifted hexagon cell $\Omega_j$ containing two half-cylinders and the nearby regular hexagon cell $\tilde{\Omega}_j$. Here, $\tilde{\Omega}_j$ is obtained by translating the left half of $\Omega_j$ horizontally by the distance $a$.

$M_j$ directly from the reduced DtN map $\tilde{M}_j$ of a regular cell $\tilde{\Omega}_j$ that contains one cylinder. As shown in Fig. 4, the cell $\tilde{\Omega}_j$ is obtained by translating the left half of $\Omega_j$ horizontally by the distance $a$ to the right. Assuming that the original cell $\Omega_j$ is bounded horizontally by $0 < x < a$, it is clear that the top boundaries of $\Omega_j$ and $\tilde{\Omega}_j$, i.e., $\Gamma_j$ and $\tilde{\Gamma}_j$, share one common edge corresponding to $a/2 < x < a$, and the second edge of $\tilde{\Gamma}_j$ is a horizontal translation of the first edge of $\Gamma_j$. If we separate the wave field on $\Gamma_j$ and $\tilde{\Gamma}_j$ following the edges and make use of the quasi-periodic condition, then

$$u_j = \begin{bmatrix} u_j^{(1)} \\ u_j^{(2)} \end{bmatrix}, \quad \tilde{u}_j = \begin{bmatrix} u_j^{(2)} \\ \rho u_j^{(1)} \end{bmatrix} = T_j u_j, \quad T_j = \begin{bmatrix} 0 & I \\ \rho I & 0 \end{bmatrix},$$

where $u_j^{(1)}$ and $u_j^{(2)}$ denote $u$ on the first and second edges of $\Gamma_j$, corresponding to $0 < x < a/2$ and $a/2 < x < a$, respectively, $I$ is the identity matrix compatible with the column vectors $u_j^{(1)}$ and $u_j^{(2)}$. Since the corner points are not used in our matrix approximations of the DtN maps, the vectors $u_j^{(1)}$ and $u_j^{(2)}$ are uniquely defined. Similarly, on the lower boundaries $\Gamma_{j-1}$ and $\tilde{\Gamma}_{j-1}$, we have a matrix $T_{j-1}$, such that $\tilde{u}_{j-1} = T_{j-1} u_{j-1}$. Since the quasi-periodic condition is also applicable to the normal derivative of $u$, we have $\partial_\nu \tilde{u}_l = T_l \partial_\nu u_l$ for $l = j-1$ and $l = j$. The reduced DtN map of $\tilde{\Omega}_j$ gives us

$$\tilde{M}_j \begin{bmatrix} \tilde{u}_{j-1} \\ \tilde{u}_j \end{bmatrix} = \begin{bmatrix} \tilde{M}_{11} & \tilde{M}_{12} \\ \tilde{M}_{21} & \tilde{M}_{22} \end{bmatrix} \begin{bmatrix} \tilde{u}_{j-1} \\ \tilde{u}_j \end{bmatrix} = \begin{bmatrix} \partial_\nu \tilde{u}_{j-1} \\ \partial_\nu \tilde{u}_j \end{bmatrix}.$$

This leads to

$$M_j = \begin{bmatrix} T_{j-1} & \\ & T_j \end{bmatrix}^{-1} \tilde{M}_j \begin{bmatrix} T_{j-1} & \\ & T_j \end{bmatrix}.$$

For the blocks of $M_j$, we have

$$M_{11} = T_{j-1}^{-1} \tilde{M}_{11} T_{j-1}, \quad M_{12} = T_{j-1}^{-1} \tilde{M}_{12} T_j, \quad M_{21} = T_j^{-1} \tilde{M}_{21} T_{j-1}, \quad M_{22} = T_j^{-1} \tilde{M}_{22} T_j.$$

## 5. Numerical examples

In this section, we illustrate our method by a few numerical examples. The first example was originally analyzed by Sakoda [18] using a plane wave expansion method. It consists of arrays of air-holes in a background dielectric medium with a refractive index $n_2 = \sqrt{2.72}$. The air-holes are given in a triangular lattice with lattice constant $a$ and the radius of the air-holes is $r = 0.431a$. The case with 4 arrays is shown in Fig. 5. As in section 2, the structure is

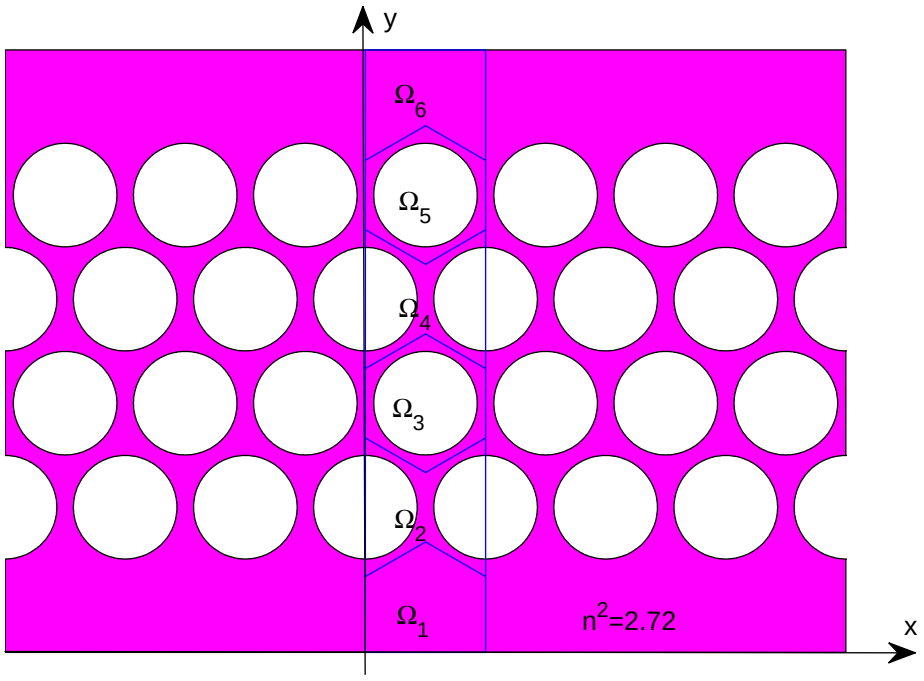


Fig. 5. Four layers of air-holes in a dielectric medium with $n = \sqrt{2.72}$. The structure is surrounded by air. The domain $S$ covering one period of the structure in the horizontal direction is divided into 6 cells.

periodic in the $x$ direction with period $a$ and is finite in the $y$ direction. The distance from the boundary of the background medium to the surfaces of the out-most air-holes is $0.778a$. The medium above and below the structure is air. Since $r < (\sqrt{3}/4)a$, the air-hole arrays do not interpenetrate, therefore the DtN-map method based on rectangular cells is applicable [14]. We include this example here to validate the improved DtN-map method developed in this paper. The domain $S$ given by $0 < x < a$ and $0 < y < D$, where $D$ is the total thickness of the structure in the $y$ direction, is divided into $m$ cells $\Omega_j$ for $1 \leq j \leq m$. The first and

last cells $\Omega_1$ and $\Omega_m$ are polygon cells bounded by the dielectric-air interfaces at $y = 0$ and $y = D$, respectively. These two cells do not have air-holes, but their reduced DtN maps can be easily calculated by the method described in section 4. For the case with 14 arrays of air-holes ($m = 16$), we calculate the transmission and reflection spectra for plane incident waves at normal incidence. Part of the transmission spectrum is shown in Fig. 6, where two

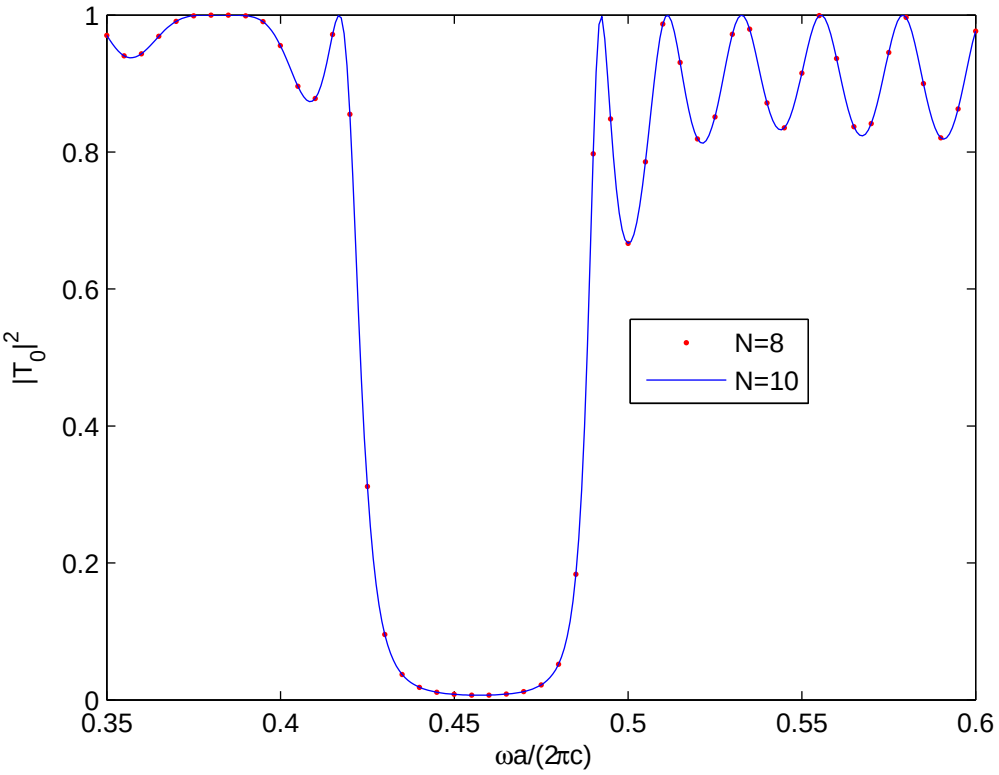


Fig. 6. Transmission spectrum obtained using the improved DtN-map method for 14 arrays of air-holes in a dielectric medium. Here, $T_0$ is the transmission coefficient defined in Eq. (3).

numerical solutions obtained using different values of $N$ (the number of sampling points on each edge of the hexagon unit cells) are compared. Our results are in excellent agreement with those in [18] and [14]. In fact, we have attempted to plot the solutions obtained with the earlier DtN-map method using rectangular unit cells [14] on top of Fig. 6, but the difference is much smaller than the line width. For a number of frequencies, we checked the numerical convergence of our method. The relative errors appear to decrease exponentially as $N$ is increased.

For the second example, we consider dielectric cylinders with refractive index $n_1 = \sqrt{11.4}$

given in a triangular lattice where the background medium is air. Using the notations of section 2 and Fig. 1, we have $n_2 = n_{top} = n_{bot} = 1$. The structure consists of $m = 15$ layers of circular cylinders in the $y$ direction. As in Fig. 1, the domain $S$ corresponding to one period of the structure in the $x$ direction is divided into 15 cells. The first and last cells are polygons similar to those in Fig. 2 (middle and right).

First, we consider plane incident waves at normal incidence in the $E$ polarization. For cylinders with radius $r = 0.45a$, we obtain the transmission spectrum shown in Fig. 7. Using the MIT Photonic-Bands package [19] with 128 plane waves for each lattice constant, we obtain the first 5 bandgaps shown as the yellow vertical strips in Fig. 7. These results also confirm the gap map calculated by the DtN-map method in [17]. While the bandgaps correspond to the non-existence of propagating Bloch mode in any direction, for normal incident waves, the partial gaps assuming the Bloch wave vector is restricted to the $\Gamma M$ edge of the irreducible Brillouin zone are more relevant, where $\Gamma = (0, 0)$ and $M = (0, 2\pi/(\sqrt{3}a))$. The first bandgap, $0.2020 < \omega a/(2\pi c) < 0.2068$, is quite small, but the corresponding partial gap is larger: $0.1827 < \omega a/(2\pi c) < 0.2068$. In Fig. 7, the starting point of the first partial gap is shown as the vertical dashed line. In general, low transmission is observed for frequencies in the bandgaps (or partial gaps). However, the transmission coefficient in the first bandgap is not so small. In fact, $|T_0|$ is about 0.41 for $\omega a/(2\pi c) = 0.205$. This may be related to the fact that the frequency is quite small, the wavelength is long, so the 15 layers of cylinders are not sufficient to block the incident wave. With 31 layers, we found that $|T_0|$ is less than 0.08 at the same frequency. In Fig. 7, there are other low transmission intervals outside the bandgaps and even the partial gaps. A symmetry mismatch between the incident wave and the propagating Bloch mode may cause the low transmission in these intervals.

To test the convergence, we calculate the relative errors of the zeroth order reflection coefficient $R_0$ for difference values of $N$, where $N$ is the number of sampling points on each edge of the hexagon unit cells. The reference solution obtained with $N = 20$ is used to define the relative errors for smaller values of $N$. In Fig. 8, we show the relative errors of $R_0$ for $\omega a/(2\pi c) = 0.3$ and 0.8. Good convergence rates are obtained for both frequencies. A faster convergence is observed for the lower frequency, since the wave field is smoother in that case. For the $E$ polarization, our method works even when the cylinders touch each other, i.e., $r = 0.5a$. In Fig. 9, we show the transmission spectrum for $r = 0.5a$ and normal incident waves. Although the wave field is quite complicated near the contacting points, our method still converges as $N$ is increased. In Fig. 10 (left), we show the zeroth order reflection coefficient $R_0$ calculated with different values of $N$ at $\omega a/(2\pi c) = 0.3$. For this example, we also consider the $H$ polarization. In that case, when $r$ is close to $0.5a$, the wave field between two nearby cylinders is even more complicated, since the normal derivative of $u$ is not continuous on the cylinder surfaces. Nevertheless, our method converges for $r < 0.5a$.

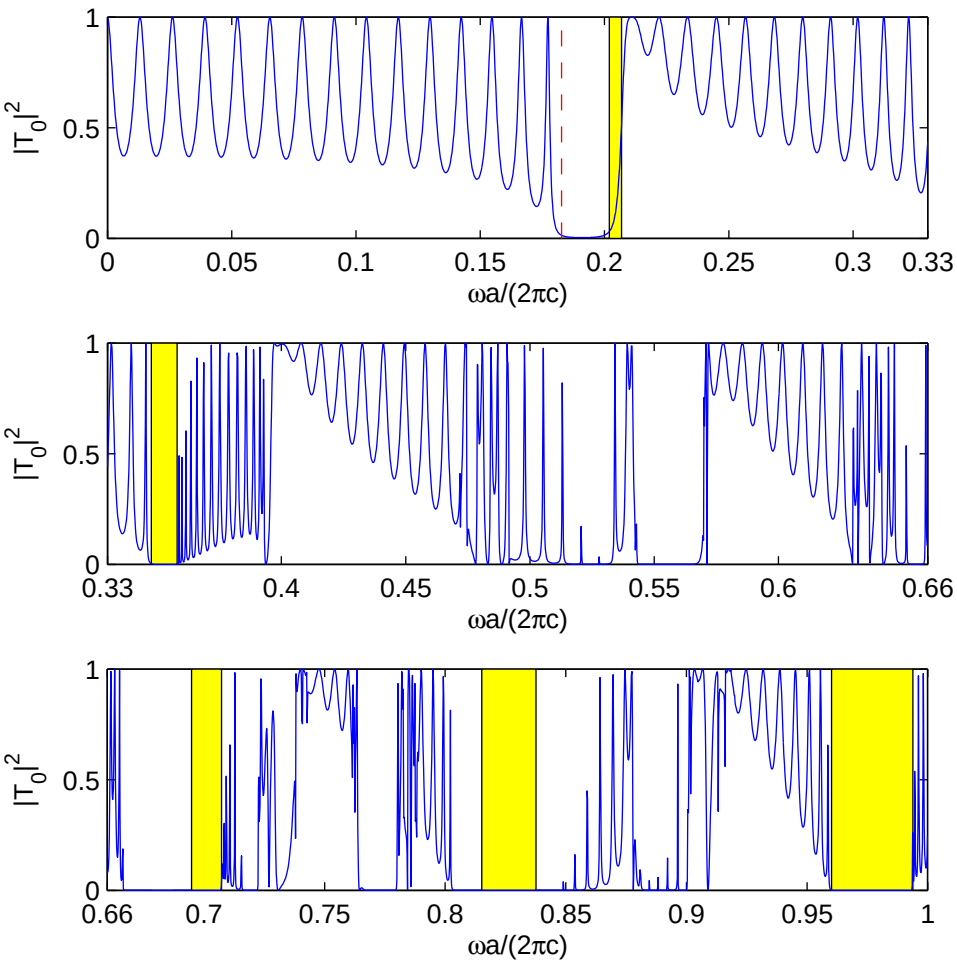


Fig. 7. Transmission spectrum of 15-layers of dielectric cylinders with radius $r = 0.45a$ for the $E$ polarization. The bandgaps of the bulk PhC are shown as the yellow vertical strips. The vertical dashed line indicates the starting point of the first partial gap obtained by assuming that the Bloch wave vector is restricted to the $\Gamma M$ edge of the first Brillouin zone.

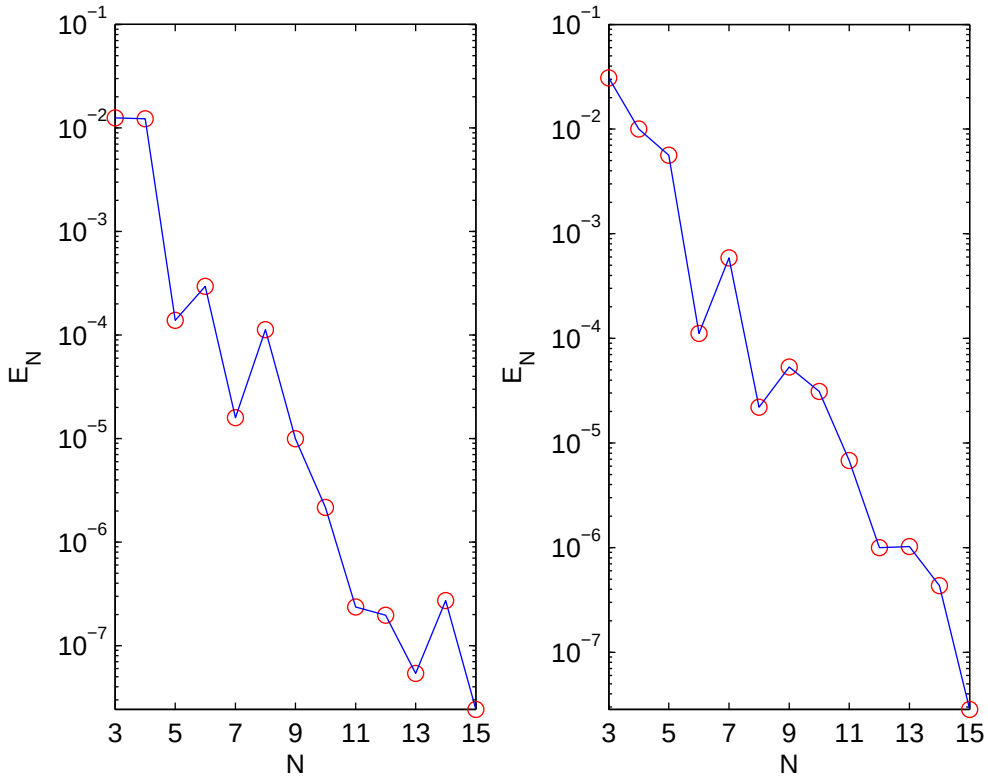


Fig. 8. Relative errors of the reflection coefficient $R_0$ versus $N$ for 15 layers of dielectric cylinders with radius $r = 0.45a$ and the $E$ polarization. The frequencies are $\omega a/(2\pi c) = 0.3$ (left) and $\omega a/(2\pi c) = 0.8$ (right).

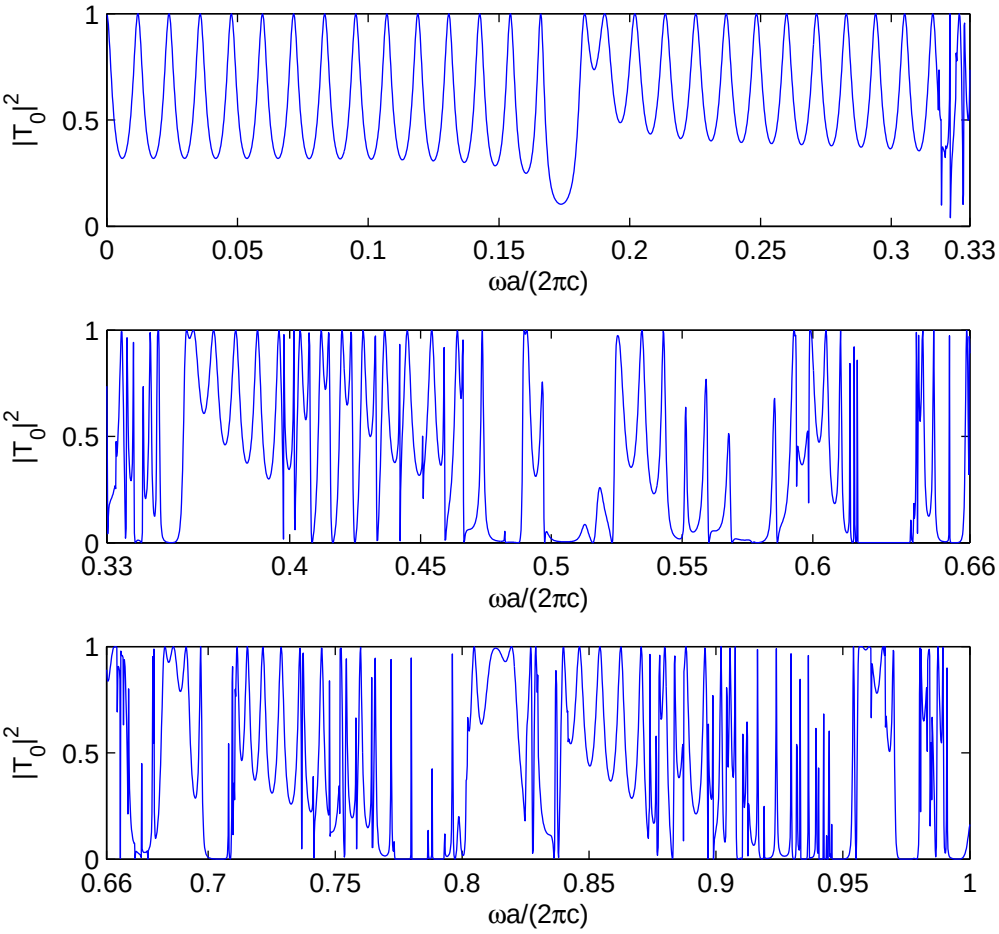


Fig. 9. Transmission spectrum of 15-layers of dielectric cylinders with radius $r = 0.5a$ for the $E$ polarization.

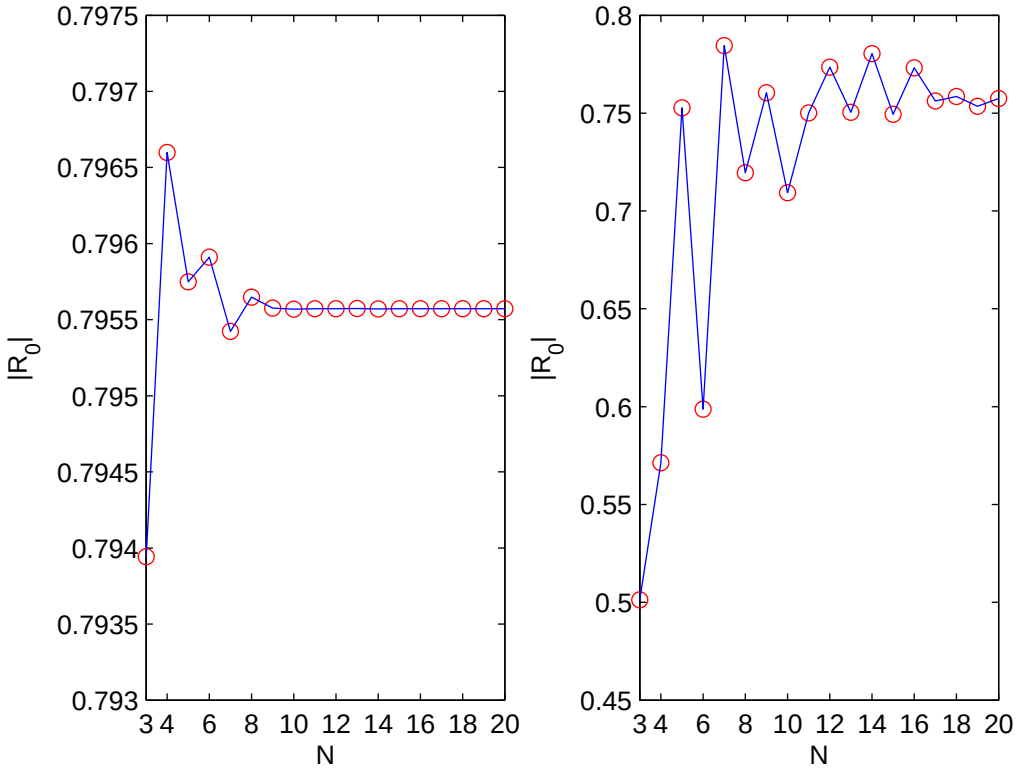


Fig. 10. Zeroth order reflection coefficient $R_0$ verses $N$ for 15 layers of cylinders and $\omega a/(2\pi c) = 0.3$. Left: $E$ polarization and $r = 0.5a$; Right: $H$ polarization and $r = 0.49a$.

In Fig. 10 (right), we show the reflection coefficient $R_0$ obtained with different values of $N$ for $r = 0.49a$ and $\omega a/(2\pi c) = 0.3$. However, our method fails to converge when $r = 0.5a$ for the $H$ polarization.

As a third example, we analyze transmission and reflection spectra for plane waves incident upon perfectly electric conductor (PEC) cylinders in free space. First, we consider one array of PEC cylinders. In Fig. 11, we show the reflection spectra for a few different values of the

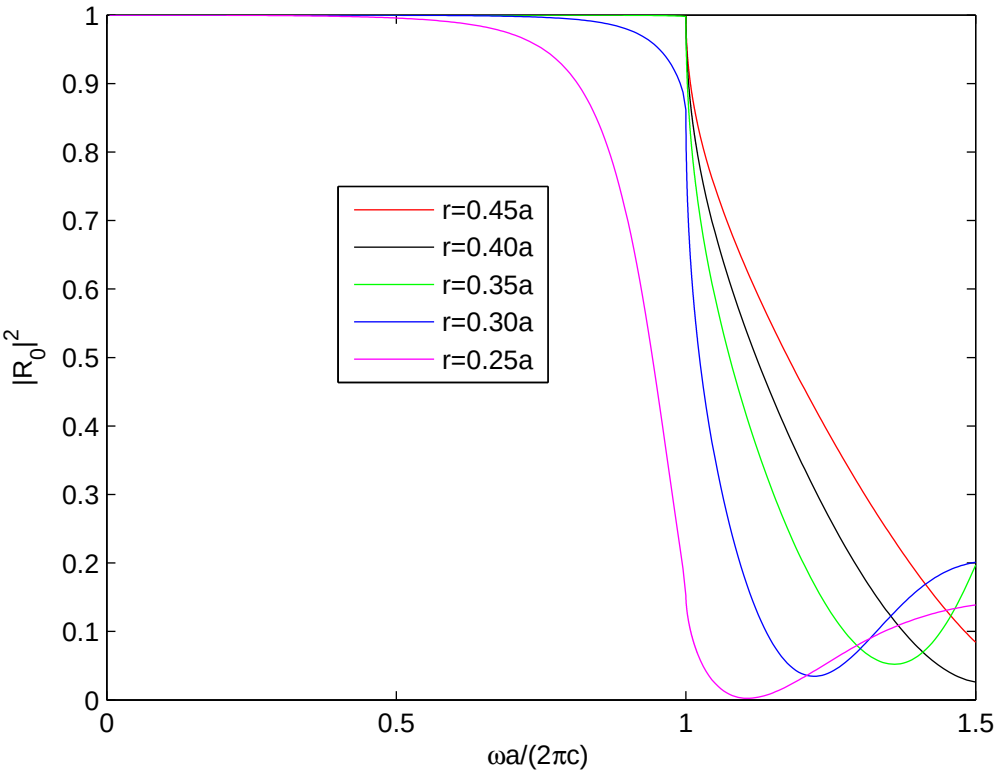


Fig. 11. Reflection spectra of one layer of PEC cylinders for the $E$ polarization and different values of the cylinder radius $r$.

cylinder radius $r$. These are results for normal incident plane waves in the $E$ polarization. For larger values of $r$, the zeroth order reflection coefficient $R_0$ nearly satisfies $|R_0| = 1$ for $\omega a/(2\pi c) < 1$ and it decays rapidly as the frequency is further increased. Notice that if $\omega a/(2\pi c) < 1$, then the zeroth order diffraction mode is the only propagating mode. If $\omega a/(2\pi c) > 1$, then $\beta_1$ and $\beta_{-1}$ (as in Eq. (2)) are real, the diffraction modes of order $\pm 1$ become propagating and the power of the incident wave can also be coupled to these modes. Next, we consider $m = 15$ layers of PEC cylinders given in a triangular lattice. For the $H$ polarization and normal incident plane waves, we obtain the transmission spectrum in

Fig. 12. Two frequency intervals where $T_0$ is nearly zero are observed for $\omega a/(2\pi c) < 1$.

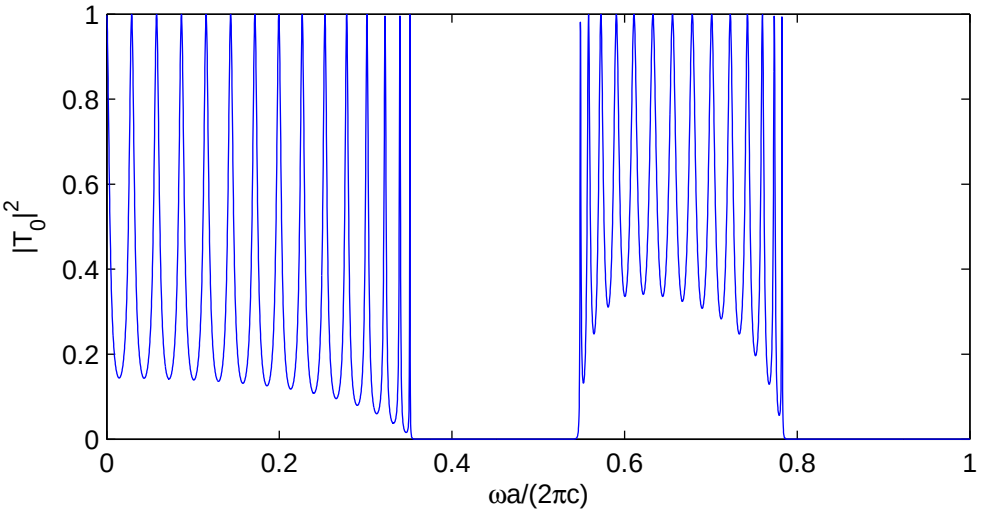


Fig. 12. Transmission spectrum of 15 layers of PEC cylinders in a triangular lattice for normal incident plane waves in the $H$ polarization. The radius of the cylinders is $r = 0.45a$.

## 6. Conclusions

In this paper, we developed an improved Dirichlet-to-Neumann (DtN) map method for computing transmission and reflection spectra of finite two-dimensional photonic crystals (PhCs) composed of cylinders in a triangular lattice. Our method is particularly efficient for analyzing PhCs with interpenetrating layers, where the ratio between the radius $r$ of the cylinders and the lattice constant $a$ is greater than $\sqrt{3}/4$. Some existing numerical methods based on considering a finite PhC as a multilayer grating stack, such as the multipole method [8] and the previous DtN-map method [14], have difficulties for PhCs with interpenetrating layers. Our method relies on manipulating some operators defined on curves and these operators can be approximated by small matrices. In particular, the DtN maps of the unit cells (hexagon unit cells and special polygon cells near the boundaries) allow us to avoid further calculations in the interiors of the unit cells. Our method is illustrated by a number of numerical examples including air-holes in a dielectric background medium, and dielectric and perfect electric conductor cylinders in vacuum. The method is applicable to structures involving real metals for which the dielectric constant is complex. The current implementation is limited to two-dimensional structures with infinitely long and parallel cylinders and for waves propagating in the plane transverse to the cylinder axes. The method is being extended to cases

involving oblique incident waves.

**Acknowledgments**

This research was partially supported by a grant from the Research Grants Council of Hong Kong Special Administrative Region, China (Project No. CityU 101706).

Yumao Wu's e-mail address is ymwu@mail.ustc.edu.cn, Ya Yan Lu's e-mail address is mayylu@cityu.edu.hk.

**References**

1. J. D. Joannopoulos, R. D. Meade and J. N. Winn, *Photonic Crystals: Molding the Flow of Light*, (Princeton University Press, Princeton, NJ. 1995).
2. G. Bao, D. C. Dobson and J. A. Cox, "Mathematical studies in rigorous grating theory", J. Opt. Soc. Am. A **12**, 1029-1042 (1995).
3. P. Lalanne and G. M. Morris, "Highly improved convergence of the coupled-wave method for TM polarization", J. Opt. Soc. Am. A **13**, 779-784 (1996).
4. L. Li, "Formulation and comparison of two recursive matrix algorithms for modeling layered diffraction gratings", J. Opt. Soc. Am. A **13**, 1024-1035 (1996).
5. G. Bao Z. M. Chen and H. J. Wu, "Adaptive finite-element method for diffraction gratings", J. Opt. Soc. Am. A **22**, 1106-1114 (2005).
6. S. Venakides, M. A. Haider and V. Papanicolaou, "Boundary integral calculations of two-dimensional electromagnetic scattering by photonic crystal Fabry-Perot structures", SIAM Journal on Applied Mathematics **60**, 1686-1706 (2000).
7. R. C. McPhedran, L. C. Botten, A. A. Asatryan, et al., "Calculation of electromagnetic properties of regular and random arrays of metallic and dielectric cylinders", Phys. Rev. E **60**, 7614-7617 (1999).
8. L. C. Botten, N. A. Nicorovici, A. A. Asatryan, et al., "Formulation for electromagnetic scattering and propagation through grating stacks of metallic and dielectric cylinders for photonic crystal calculations. Part I. Method", J. Opt. Soc. Am. A **17**, 2165-2176 (2000).
9. T. Kushta and K. Yasumoto, "Electromagnetic scattering from periodic arrays of two circular cylinders per unit cell," Progress In Electromagnetics Research **29**, 69-85 (2000).
10. L. C. Botten, T. P. White, A. A. Asatryan, et al., "Bloch mode scattering matrix methods for modeling extended photonic crystal structures. I. Theory", Phys. Rev. E **70**, 056606 (2004).
11. K. Yasumoto, H. Toyama and T. Kushta, "Accurate analysis of two-dimensional electromagnetic scattering from multilaye red periodic arrays of circular cylinders using lattice sums technique", IEEE Transactions on Antennas and Propagation **52**, 2603-2611 (2004).

12. K. Yasumoto, H. Jia and H. Toyama, "Analysis of two-dimensional electromagnetic crystals consisting of multilayered periodic arrays of circular cylinders", Electronics and Communications in Japan, Part II – Electronics **88**, 19-28 (2005).
13. Y. Huang and Y. Y. Lu, "Scattering from periodic arrays of cylinders by Dirichlet-to-Neumann maps", J. Lightw. Technol. **24**, 3448-3453 (2006).
14. Y. Huang and Y. Y. Lu, "Modeling photonic crystals with complex unit cells by Dirichlet-to-Neumann maps", J. Comput. Math. **25**, 337-349 (2007).
15. S. J. Li and Y. Y. Lu, "Multipole Dirichlet-to-Neumann map method for photonic crystals with complex unit cells", J. Opt. Soc. Am. A **24**, 2438-2442 (2007).
16. L. C. Botten, N. A. Nicorovici, R. C. McPhedran, C. M. de Sterke and A. A. Asatryan, "Photonic band structure calculations using scattering matrices," Phys. Rev. E **64**, 046603, 2001.
17. J. Yuan and Y. Y. Lu, "Computing photonic band structures by Dirichlet-to-Neumann maps: The triangular lattice" , Opt. Commun. **273**, 114-120 (2007).
18. K. Sakoda, "Optical transmittance of a two-dimensional triangular photonic lattice", Phys. Rev. B **51**, 4672-4675 (1995).
19. S. G. Johnson and J. D. Joannopoulos, "Block-iterative frequency-domain methods for Maxwell's equations in a planewave basis", Opt. Express **8**, 173-190 (2001).